Proc. Natl. Acad. Sci. USA
Vol. 91, pp. 10193–10197, October 1994
Medical Sciences

In vivo diagnosis of cervical intraepithelial neoplasia using 337-nm-excited laser-induced fluorescence

N. RAMANUJAM*, M. F. MITCHELL†, A. MAHADEVAN*, S. WARREN*, S. THOMSEN‡, E. SILVA‡, AND R. RICHARDS-KORTUM*§

*Biomedical Engineering Program, University of Texas, Austin, TX 78712; and Departments of †Gynecology and ‡Pathology, University of Texas M. D. Anderson Cancer Center, Houston, TX 77030

Communicated by Britton Chance, June 2, 1994 (received for review June 25, 1993)

ABSTRACT **Laser-induced fluorescence at 337-nm excitation was used *in vivo* to differentiate neoplastic [cervical intraepithelial neoplasia (CIN)], nonneoplastic abnormal (inflammation and human papilloma viral infection), and normal cervical tissues. A colposcope (low-magnification microscope used to view the cervix with reflected light) was used to identify 66 normal and 49 abnormal (5 inflammation, 21 human papilloma virus infection, and 23 CIN) sites on the cervix in 28 patients. These sites were then interrogated spectroscopically. A two-stage algorithm was developed to diagnose CIN. The first stage differentiated histologically abnormal tissues from colposcopically normal tissues with a sensitivity, specificity, and positive predictive value of 92%, 90%, and 88%, respectively. The second stage differentiated preneoplastic and neoplastic tissues from nonneoplastic abnormal tissues with a sensitivity, specificity, and positive predictive value of 87%, 73%, and 74%, respectively. Spectroscopic differences were consistent with a decrease in the absolute contribution of collagen fluorescence, an increase in the absolute contribution of oxyhemoglobin attenuation, and an increase in the relative contribution of reduced nicotinamide dinucleotide phosphate [NAD(P)H] fluorescence as tissue progresses from normal to abnormal in the same patient. These results suggest that *in vivo* fluorescence spectroscopy of the cervix can be used to diagnose CIN at colposcopy.**

Although there has been a significant decline in the incidence and mortality of invasive cervical cancer in the last 50 years (1), there has been an increase in the incidence of cervical intraepithelial neoplasia (CIN), reflecting both improved screening and detection methods and a true increase in the incidence of precancerous lesions of the cervix (2). The mortality of cervical cancer is estimated to rise by 20% in the years 2000–2004 unless improvements are made in current screening and detection techniques (3). Initial screening for cervical cancer and CIN requires a cytologic smear. A false-negative error rate of 20–30% is associated with this technique due to insufficient sampling and reading error (4). An abnormal Papanicolaou (Pap) smear is followed by colposcopy, biopsy, histologic evaluation, and diagnosis (5). The accuracy of colposcopy in differentiating human papilloma viral (HPV) infection and CIN from normal and inflammatory cervical tissues is variable and limited even in experienced hands [average sensitivity, specificity, and positive predictive value (6) of 94% ± 14%, 51% ± 24%, and 83% ± 15%, respectively (7)]. A method to improve the performance of colposcopy could save patients from multiple biopsies, allow more effective wide-scale diagnosis, and potentially permit combined diagnosis and treatment in a single visit.

Spectroscopic methods show potential for differentiating cervical neoplasia from the normal cervix (8–11). At 330-nm excitation, the steady-state fluorescence of abnormal tissue is significantly weaker than that of normal tissue from the same patient *in vitro* (8). An algorithm to identify histologic abnormality based on comparison of peak intensities of histologically normal and abnormal biopsies from the same patient had a sensitivity, specificity, and positive predictive value of 75%, 88%, and 86%, respectively (8).

Fluorescence spectra have been measured *in vivo* to detect neoplastic tissues in a variety of organ systems (12–14). Lam *et al.* (12) demonstrated that the sensitivity of fluorescence bronchoscopy is greater than conventional bronchoscopy. Autofluorescence has also been used to distinguish adenomatous polyps from normal colon and hyperplastic polyps *in vivo* (13, 14). To quantitate spectral changes, Schomacker (14) fit fluorescence spectra of colonic tissue (337-nm excitation) to a linear combination of three fluorescent components: collagen, reduced nicotinamide adenine dinucleotide (NADH), and flavin adenine dinucleotide (FAD). Good fits were obtained except over 400–440 nm and 520–600 nm, where hemoglobin reabsorption is greatest. A decrease in collagen fluorescence and an increase in NADH fluorescence and hemoglobin reabsorption were seen as tissue progresses from normal to adenocarcinoma.

These studies indicate the potential of fluorescence to diagnose neoplasia. Algorithms are implemented in software and can potentially place automated cancer detection in the hands of less experienced practitioners. A quantitative analysis of fluorescence spectra to obtain contributions of individual tissue components can provide insight into biochemical changes associated with neoplasia.

On the basis of the spectroscopic differences between normal, nonneoplastic abnormal, and neoplastic cervical tissue *in vitro* and the capability to measure tissue fluorescence rapidly *in vivo*, we designed a study to measure autofluorescence of the intact cervix at colposcopy. Our goal was to develop and evaluate the performance of a spectroscopic method to differentiate CIN from normal and nonneoplastic abnormal cervical tissues. A preliminary analysis of fluorescence data acquired *in vivo* from 28 patients indicated that peak fluorescence intensities of histologically abnormal tissues are statistically less than that of colposcopically normal tissues in the same patient (15). In addition, spectral line shapes are statistically different between 400 and 450 nm. An algorithm was developed to differentiate histologic abnormality from colposcopically normal tissues with a high sensitivity, specificity, and positive predictive value (15). However, this preliminary analysis had two important limitations: clinically, the differential diagnosis of CIN and HPV infection is needed to determine if therapy is required. Furthermore, it is necessary to understand the biochemical and morphologic basis of the spectroscopic algorithms to appreciate additional informa-

The publication costs of this article were defrayed in part by page charge payment. This article must therefore be hereby marked "*advertisement*" in accordance with 18 U.S.C. §1734 solely to indicate this fact.

Abbreviations: CIN, cervical intraepithelial neoplasia; HPV, human papilloma virus.

§To whom reprint requests should be addressed.

tion that may be available and to predict clinical conditions in which its diagnostic ability may be limited.

This paper describes a clinical study and data analysis method to address these limitations. A two-stage spectroscopic algorithm to diagnose histologic abnormality and differentially diagnose CIN at colposcopy is presented. Spectra acquired *in vivo* are compared to those reported *in vitro* (8) to assess the utility of *in vitro* studies. Finally, to investigate the biochemical and morphologic basis of the spectroscopic signatures of different tissues, spectra acquired *in vivo* are fit to a model of turbid tissue fluorescence.

MATERIALS AND METHODS

Instrumentation. A spectroscopic system incorporating a pulsed nitrogen laser, an optical fiber probe, and an optical multichannel analyzer was used to record fluorescence spectra of sites on the cervix *in vivo* (15). The laser characteristics for this study were 337-nm wavelength, 5-ns pulse duration, 40-Hz repetition rate, and a transmitted pulse energy of 70 μJ.

Fluorescence Measurements of the Cervix. Patients were selected from a group referred for colposcopy on the basis of abnormal cervical cytology. Informed consent was obtained and study was reviewed and approved by the Internal Review Boards of the University of Texas at Austin and the University of Texas M. D. Anderson Cancer Center. In each patient, after colposcopic evaluation (5) but before biopsy, the rigid end of the fluorescence probe was inserted into the vagina under colposcopic control until the tip was in contact with tissue. Fifteen fluorescence spectra were then acquired from the area directly illuminated by the probe during consecutive laser pulses. Between each patient study, the probe was disinfected for 20 min in Metricide (Metrex Research) to prevent transmission of the human immunodeficiency virus. On average, spectra from two abnormal sites and two normal sites were obtained per patient. Abnormal sites analyzed by the probe were biopsied. Histologic examination was performed using the standard classification scheme for identification of inflammation, HPV infection, and CIN (2). All spectra were corrected for nonuniform spectral response of the detection system by using correction factors obtained with an N.I.S.T. traceable calibration lamp. The average spectrum from each cervical site was calculated and normalized to the peak intensity of a standard (15); absolute fluorescence intensities are reported in these calibrated units.

Fluorescence Measurements of Pure Fluorophores. Potential chromophores contributing to cervical tissue fluorescence were identified from the literature (8, 9, 11, 13, 14). Fluorescence spectra of optically dilute solutions of human collagen type I (1 mg/ml; Sigma, C4407), human elastin (1 mg/ml; Elastin Products, St. Louis, SH476), NADH (0.025 mM; Kodak, 136 7767), and FAD (0.01 mM; Kodak, 136 8422) in phosphate-buffered saline (pH 7.4, P_{O_2} = 160 mmHg) were obtained at 337-nm excitation, 350- to 700-nm emission, using the same instrument for measuring fluorescence of the cervix. The normalized fluorescence line shapes of all chromophores in solution were used in subsequent analysis. The absorbance of oxyhemoglobin in fresh human blood was recorded using an absorption spectrophotometer.

Least Squares Fit. Tissue spectra were fit to a model of turbid tissue fluorescence (Eq. 1; ref. 16) to extract the contributions of tissue chromophores.

$$S(\lambda_{em}) = \frac{C_1C(\lambda_{em}) + C_2E(\lambda_{em}) + C_3N(\lambda_{em}) + C_4F(\lambda_{em})}{C_5[A(\lambda_{exc}) + A(\lambda_{em})] + C_6}. \quad [1]$$

Here, $S(\lambda_{em})$ represents fluorescence intensity as a function of emission wavelength (λ_{em}) in calibrated units; $C(\lambda_{em})$, $E(\lambda_{em})$, $N(\lambda_{em})$, and $F(\lambda_{em})$ represent the normalized fluorescence spectra of collagen, elastin, NAD(P)H, and FAD, respectively; and C_1–C_4 indicate the absolute contribution of each fluorophore to the tissue spectrum. This contribution is proportional to the concentration, peak quantum yield, and depth distribution of the fluorophore. The denominator includes the normalized sum of oxyhemoglobin attenuation at the excitation and emission wavelengths [$A(\lambda_{exc}) + A(\lambda_{em})$] with contribution C_5. A broad band attenuation is represented by C_6. This model of turbid tissue fluorescence assumes that light is attenuated exponentially (due to absorption and scattering) in a homogeneous, optically thick tissue (16). Cervical tissue emission spectra were fit to Eq. 1 in the least squares sense with C_1–C_5 as free parameters of the fit subject to the constraints C_1–$C_5 > 0$. To establish a scale for the coefficients C_1–C_5, C_6 was set to 1 in the fitting process; C_1–C_5 are reported relative to C_6.

RESULTS

Fluorescence spectra were recorded from 115 cervical sites in 28 women. The mean age of the patients was 24 ± 6 years. Twelve of the patients were Caucasian, 11 were Black, and 5 were Hispanic. Sixty six colposcopically normal areas and 49 histologically abnormal areas (5 inflammation, 21 HPV infection, 9 CIN I, 10 CIN II, 4 CIN III, listed in order of increasing abnormality) were examined. In cases where biopsies had multiple diagnoses, sample classification was based on the most severe pathologic finding. In this initial clinical trial all colposcopically normal tissues were assumed to be histologically normal. The false-negative error rate of colposcopy indicates the percentage of colposcopically normal tissues that are histologically abnormal. This value is reported to be 12% ± 10% (7).

Typical Spectra. Fig. 1 illustrates average spectra per site acquired from all normal and abnormal cervical sites in four typical patients. All fluorescence intensities are reported in the same set of calibrated units. Error bars indicate the uncertainty (±3%) associated with the peak intensity of the spectrum with the maximum intensity from each patient and are representative of those calculated for all spectra. In all

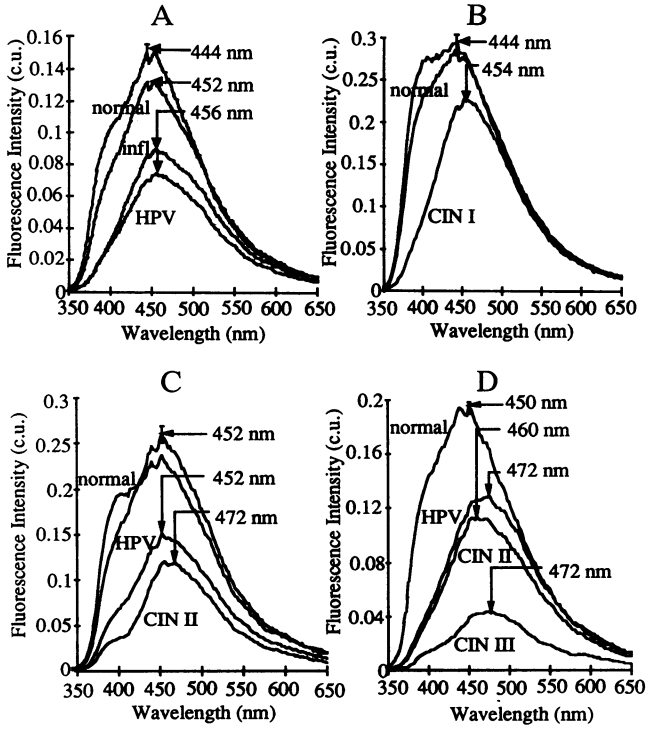

FIG. 1. Fluorescence spectra of cervical tissues from four typical patients. In each case, fluorescence intensities are reported in the same set of calibrated units (c.u.). infl, Inflammation.

four patients, the fluorescence intensities of histologically abnormal tissues are lower than those of corresponding colposcopically normal tissues. Fig. 1 indicates that the fluorescence intensities of normal tissues vary by more than a factor of two from patient to patient, while within a single patient fluorescence intensities of normal areas vary by <15%. Evaluation of abnormal tissue spectra from the same patient indicates that tissues with HPV infection are less fluorescent than tissues with chronic inflammation (Fig. 1*A*). Tissues with dysplastic changes have a lower fluorescence intensity than tissues with inflammation or HPV infection (Fig. 1*C*), with CIN III exhibiting the weakest fluorescence intensity (Fig. 1*D*). Spectral line shapes of normal tissues vary both from patient to patient and within a patient. The wavelengths corresponding to the peak intensity of all normal spectra occur within ±3 nm of 442 or 453 nm. Peak emission wavelengths of abnormal tissues occur within ±3 nm of either 444, 454, 463, or 470 nm.

The peak emission wavelength of spectra of tissues with CIN increases as the peak emission wavelength of normal tissue spectra from the same patient increases. In Fig. 1*B* the peak emission of the normal spectrum occurs at 444 nm, while the corresponding CIN I spectrum peaks at 454 nm. In Fig. 1*C*, the normal spectrum peaks at 452 nm and the corresponding CIN II spectrum peaks at 472 nm. In Fig. 1*D*, the normal spectrum peaks at 450 nm, CIN II peaks at 460 nm, and CIN III peaks at 472 nm. A similar relationship was not observed for samples with inflammation or HPV infection.

Diagnostic Algorithms. An algorithm to differentiate colposcopically normal and histologically abnormal cervical tissue *in vivo* was developed based on differences in spectral line shape and peak fluorescence intensity. To compensate for interpatient variability in peak fluorescence intensity, fluorescence spectra of all samples were normalized to the average peak fluorescence intensity of spectra obtained from colposcopically normal sites in the same patient (relative peak fluorescence intensity). The slope of the spectrum over a given wavelength range was used to characterize spectral line shape. All spectra were normalized to a peak intensity of one prior to slope calculation. A linear approximation of spectral slope was determined over 20-nm increments: slope = $\{S[(\lambda_{em} + 20\text{ nm}) - S(\lambda_{em})]/20\text{ nm}\}$. Greatest differences in the slope of normal and abnormal tissue spectra occur over the wavelength range 420–440 nm.

A two-dimensional scatter plot of the slope from 420 to 440 nm versus the relative peak fluorescence intensity of each site is shown in Fig. 2. The relative peak fluorescence intensities of colposcopically normal samples are close to 1 while the relative peak fluorescence intensities of histologically abnormal sites are <1 on average. The slope over 420–440 nm of abnormal tissue spectra is greater than that of normal tissue spectra, which in part reflects the longer peak emission wavelength of abnormal tissue fluorescence. Sites that lie below the decision line in Fig. 2 are classified as normal and those that lie above the line are classified as abnormal. This algorithm diagnoses histologic abnormality with a sensitivity, specificity, and positive predictive value of 92%, 90%, and 88%, respectively. Three of the four abnormal samples misclassified have HPV infection and the fourth has CIN I. The spectroscopic algorithm classifies 9% of the colposcopically normal tissues as abnormal, comparable to the average false-negative rate (12% ± 10%) for colposcopy (7).

A spectroscopic algorithm capable of differentiating CIN from HPV infection or inflammation would be of greater clinical value. A relationship, as noted in Fig. 1 *B–D*, was observed between the peak emission wavelengths of CIN spectra and their corresponding normal spectra. This relationship was not observed in the spectra of samples with HPV infection and inflammation. Hence, a simple diagnostic algorithm based on peak emission wavelengths can be defined.

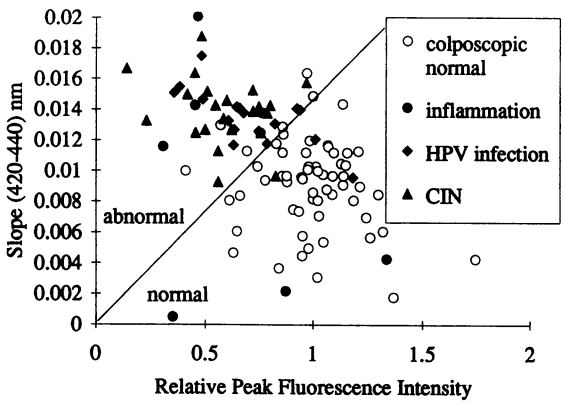

FIG. 2. Scatter plot of slope over 420–440 nm versus relative peak fluorescence intensity of normal and abnormal tissue spectra. The algorithm diagnoses abnormal tissues with a sensitivity of 92%, a specificity of 90%, and a positive predictive value of 88%.

However, because the emission peaks are broad, these values can be significantly shifted by noise. Less sensitive to noise, but still related to peak emission wavelength, is the slope of the spectrum over the peak emission wavelength range. The peak emission wavelength of normal tissues can be characterized by the slope of the spectrum from 420 to 440 nm. Normal spectra with a small positive slope value indicate a peak near 442 nm, while those with a large positive slope value correspond to a peak near 453 nm. Similarly, the peak emission wavelength of abnormal spectra can be represented by the slope from 440 to 460 nm. A negative slope indicates a peak near 444 nm, a small positive or negative slope value indicates a peak near 454 nm, and a large positive slope corresponds to a peak emission wavelength near 463–470 nm.

The relationship between the peak emission wavelength of the abnormal spectrum and normal spectra from the same patient is mapped as a two-dimensional scatter plot in Fig. 3, where the abscissa corresponds to the slope of the abnormal spectrum over the wavelength range 440–460 nm and the ordinate represents the average slope of normal spectra from the same patient over the wavelength range 420–440 nm. An algorithm to differentiate tissues with CIN from tissues with HPV infection or inflammation is represented by the decision line in Fig. 3, chosen to minimize the number of misclassified samples and maximize sensitivity. CIN is diagnosed with a sensitivity, specificity, and positive predictive value of 87%, 73%, and 74%, respectively. Two of the three CIN samples misclassified have focal CIN and HPV infection. The third

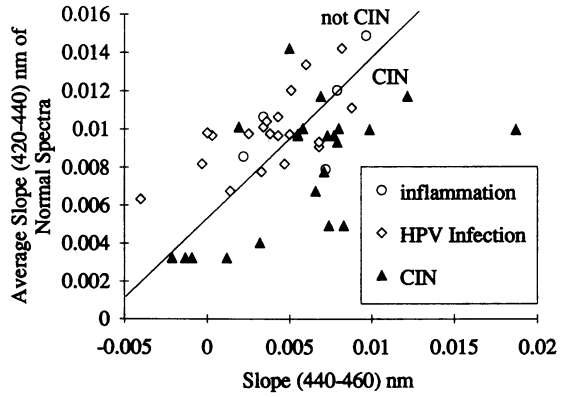

FIG. 3. Scatter plot of the average normal slope over 420–440 nm of each patient versus the slope over 440–460 nm of abnormal spectra from the same patient. The decision line diagnoses CIN with a sensitivity of 87%, a specificity of 73%, and a positive predictive value of 74%.

misdiagnosed CIN sample has CIN I and HPV infection. Six samples with HPV infection and one sample with inflammation are misclassified as CIN.

Biochemical Analysis. Four tentative fluorophores responsible for the fluorescence observed are collagen (excitation, emission maxima: 340, 410 nm) (17), NAD(P)H (excitation, emission maxima: 350, 460 nm) (18), elastin (excitation, emission maxima: 370, 415 nm) (19), and FAD (excitation, emission maxima: 450, 520 nm) (20). Fig. 4 compares measured and calculated fluorescence spectra (Eq. 1) for typical normal, HPV infection, and CIN II from the same patient. Residual differences are small and typical for all patients. Absolute contributions of tissue chromophores were determined from the average spectrum from each cervical site. Interpatient variations in spectra could not be attributed to variations in a single chromophore; therefore, to identify differences in chromophore contribution as tissue progresses from normal to abnormal within a patient, absolute contributions of chromophores were divided by the average contribution of that chromophore to normal spectra from the same patient (normalized absolute chromophore contribution). Fig. 5 *A* and *B* show the normalized absolute collagen and oxyhemoglobin contributions for all cervical sites. The absolute contribution of collagen fluorescence decreases and the contribution of oxyhemoglobin attenuation increases as tissue progresses from normal to abnormal in the same patient.

Absolute chromophore contributions reflect changes in both the intensity and shape of the fluorescence spectrum. Changes in the shape of the spectrum can be independently assessed by calculating the relative contribution of a chromophore to the spectrum. Relative contribution can be calculated by normalizing the measured spectrum to a peak intensity of 1 prior to fitting to Eq. 1. Fig. 5*C* shows the relative contribution of NAD(P)H to average spectra for the

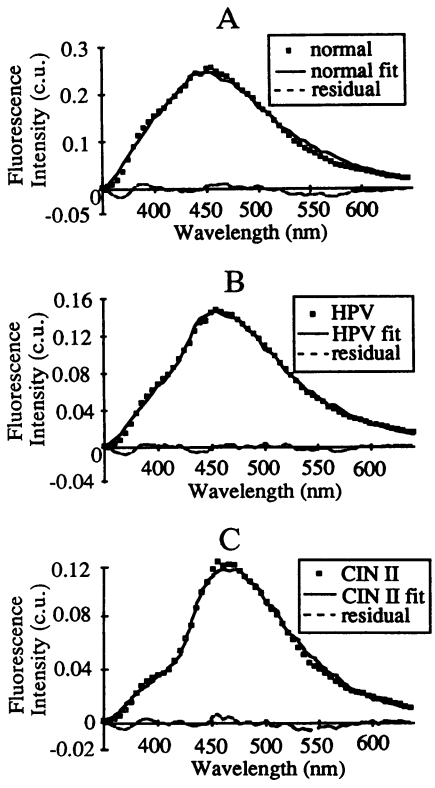

FIG. 4. Comparison of experimentally measured and calculated fluorescence spectra of normal tissue (*A*), tissue with HPV infection (*B*), and tissue with CIN II (*C*) from the same patient. The dashed line represents the residual difference between measured and calculated data. c.u., Calibrated unit.

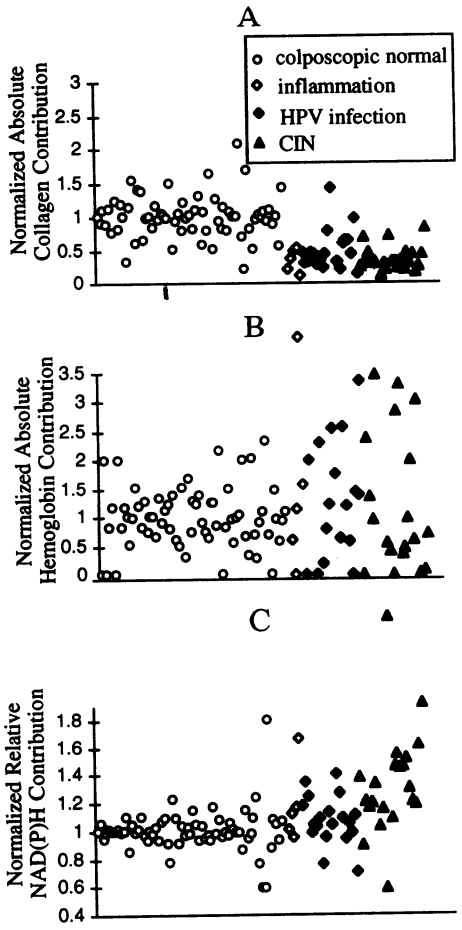

FIG. 5. Normalized absolute collagen contribution (*A*), normalized absolute oxyhemoglobin contribution (*B*), and normalized relative NAD(P)H contribution (*C*) to all 115 cervical tissue spectra.

115 cervical sites; again, contributions are divided by the average relative contribution of NAD(P)H in normal tissues from the same patient (normalized relative chromophore contribution). In general, as tissue progresses from normal to CIN in the same patient, the normalized relative contribution of NAD(P)H increases.

DISCUSSION AND CONCLUSIONS

This study indicates that a two-stage algorithm developed from laser-induced fluorescence at 337-nm excitation can be used to differentially diagnose CIN. The first stage differentiates histologically abnormal tissues from colposcopically normal tissues with a significantly improved specificity and a similar sensitivity and positive predictive value relative to colposcopy in expert hands. Unlike conventional colposcopy, the second stage of the algorithm can differentiate neoplastic from nonneoplastic abnormal tissues. In addition, this technique has the advantage of being simple to automate, potentially allowing for more wide-scale implementation of colposcopy. These advantages may ultimately circumvent the need for biopsy and further histologic analysis, enabling combined diagnosis and therapy with the loop electrosurgical procedure in a single office visit.

The *in vivo* fluorescence spectra at 337-nm excitation show several important similarities and differences from *in vitro* observations at 330-nm excitation (8). There is significant interpatient variability in the fluorescence intensity of normal tissues *in vitro* and *in vivo*, necessitating development of a paired diagnostic algorithm. Both *in vitro* and *in vivo*, the fluorescence of abnormal cervix is lower than that of normal cervix from the same patient. However, increased reabsorp-

tion effects of oxyhemoglobin are noted in spectra obtained *in vitro*, as a result of biopsy and subsequent bleeding. These differences imply that the utility of *in vitro* studies may be limited. To evaluate this, the algorithm developed to diagnose histologic abnormality *in vitro* was applied to data collected *in vivo*. The resulting specificity and positive predictive values are similar, while the sensitivity drops slightly when this algorithm is applied to *in vivo* data (Table 1). The algorithm developed for identification of histologic abnormality *in vivo* relies on both intensity and line-shape information. When this algorithm was applied to data collected *in vitro*, the sensitivity and positive predictive values dropped significantly (Table 1), confirming the limitations of *in vitro* studies for providing information about cervical tissue fluorescence line shape near 340-nm excitation.

Several hypotheses to relate differences in fluorescence spectra of normal and abnormal cervix to morphologic and biochemical differences can be developed from the least squares fit results. The squamous epithelium of the normal ectocervix has an underlying stroma that is composed mainly of collagen fibers (5). Usually neoplasia is associated with thickening of the epithelium. Hence, higher grades of neoplasia may correlate with decreased collagen fluorescence, as illustrated in Fig. 5*A* (13, 14, 21). The results of the least squares fit also demonstrate that the contribution of oxyhemoglobin appears to correlate with degree of abnormality (Fig. 5*B*). Tissues with severe grades of CIN exhibit the greatest vascularity (2). No simple correlations between the contribution of a single chromophore and the algorithm parameters could be identified; however, the results of the least squares fit can be used to develop a qualitative understanding of these algorithms. The algorithm, which differentiates histologically abnormal and colposcopically normal tissue (Fig. 2), is based on a drop in relative peak fluorescence intensity and a red shift in the peak emission wavelength as tissues become abnormal. The drop in relative peak intensity is consistent with both the drop in normalized absolute contribution of collagen fluorescence and the increase in normalized absolute contribution of oxyhemoglobin attenuation. The red shift in the peak emission wavelength is consistent with the increase in the normalized absolute contribution of oxyhemoglobin attenuation and the increase in normalized relative contribution of NAD(P)H fluorescence. The algorithm in Fig. 3 is based on the increased red shift of CIN spectra relative to normal spectra from the same patient. This is consistent with Fig. 5*C*, which demonstrates that an increase in normalized relative contribution of NAD(P)H is most prominent in samples with CIN.

Interpatient variation could not be attributed to a single constituent but may be due to the heterogeneity in the depth distribution of the different chromophores. Our study included data from samples with multiple diagnoses. For instance, tissues were classified as CIN, even if they contained only minute localized lesions. As an area 1 mm in diameter was interrogated by the probe, small localized lesions may have different fluorescence spectra. The feasibility of differentiating samples with single histologic abnormalities from those that have multiple histologic abnormalities can be investigated in studies with a larger number of patients. In addition, the signals can be correlated with the size and depth of the dysplastic lesion.

Table 1. Sensitivity (Se), specificity (Sp), and positive predictive value (PPV) of *in vitro* and *in vivo* spectroscopic algorithms applied to spectra collected *in vitro* and *in vivo*

Algorithm developed	Applied to spectra	Se, %	Sp, %	PPV, %
In vitro	*In vitro*	75	88	86
In vitro	*In vivo*	60	90	83
In vivo	*In vivo*	92	90	88
In vivo	*In vitro*	86	30	55

Future studies must also address potential limitations of algorithms presented here, which require colposcopic identification of normal tissue in each patient prior to diagnosis of histologic abnormality and CIN. Specifically, multiple sites should be spectroscopically examined on the cervix simultaneously prior to treatment with the loop electrosurgical procedure so that histologic evaluation of the excised normal and abnormal tissues can then be correlated with spectroscopic signals. The additional histologic information available from normal sites will enable evaluation of spectroscopic algorithms designed to automate detection of normal tissue. Furthermore, simultaneous interrogation of multiple sites on the cervix will allow for the evaluation of the effects of acetic acid on tissue spectra acquired prior to and at variable time intervals following the application of variable amounts of acetic acid. Finally, this protocol can be used to determine whether the sensitivity and specificity of spectroscopic diagnosis as represented here are limited by the use of colposcopy to initially identify normal and abnormal tissues.

We acknowledge the contributions of Elise Cook, M.D.; Helen Rhodes, M.D.; Lori Whitaker, M.D., Ph.D.; Judy Sandella, R.N.C., N.P., M.S.; Viho, R.N., M.S.N.; and Guillermo Tortolero-Luna, M.D., Ph.D., in the collection and analysis of clinical data. Financial support from the Whitaker Foundation is gratefully acknowledged.

1. Anderson, G. H., Boyes, D. A., Benedet, J. L., LeRiche, J. C., Matisic, J. P., Saen, K. C., Worth, N. J., Millner, A. & Bennett, O. M. (1988) *Br. Med. J.* **296**, 975–978.
2. Ferenczy, A. & Winkler, B. (1982) in *Pathology of the Female Genital Tract*, ed. Blaustein, A. (Springer, New York), pp. 156–177.
3. Beral, V. (1986) *Lancet* **i**, 495.
4. Koss, L. G. (1989) *J. Am. Med. Assoc.* **261**, 737–743.
5. Burke, L., Antonioli, D. A. & Ducatman, B. S., eds. (1991) *Colposcopy, Text and Atlas* (Appleton & Lange, Norwalk, CT).
6. Harris, E. K. & Albert, A., eds. (1987) *Multivariate Interpretation of Clinical Laboratory Data* (Dekker, New York), pp. 75–82.
7. Mitchell, M. F. (1994) *Consult. Obstet. Gynecol.* **6**, 70–73.
8. Mahadevan, A., Mitchell, M. F., Silva, E., Thomsen, S. & Richards-Kortum, R. R. (1993) *Lasers Surg. Med.* **13**, 647–655.
9. Lohmann, W., Mussmann, J., Lohmann, C. & Künzel, W. (1989) *Eur. J. Obstet. Gynecol. Reprod. Biol.* **31**, 249–253.
10. Wong, P. T. T., Wong, R. K., Caputo, T. A., Godwin, T. A. & Rigas, B. (1991) *Proc. Natl. Acad. Sci. USA* **88**, 10988–10992.
11. Glassman, W. S., Liu, C. H., Tang, G. C., Lubicz, S. & Alfano, R. R. (1992) *Lasers Life Sci.* **5**, 49–58.
12. Lam, S., Hung, J. Y. C., Kennedy, S. M., Leriche, J. C., Vedal, S., Nelems, B., Macaulay, C. E. & Palcic, B. (1992) *Am. Rev. Respir. Dis.* **146**, 1458–1461.
13. Cothren, R. M., Richards-Kortum, R. R., Sivak, M. V., Fitzmaurice, M., Rava, R. P., Boyce, G. A., Hayes, G. B., Doxtader, M., Blackman, R., Ivanc, T., Feld, M. S. & Petras, R. E. (1990) *Gastrointest. Endosc.* **36**, 105–111.
14. Schomaker, K. T., Frisoli, J. K., Compton, C. C., Flotte, T. J., Richter, J. M., Nishioka, N. S. & Deutsch, T. F. (1992) *Lasers Surg. Med.* **12**, 63–78.
15. Ramanujam, N., Mitchell, M. F., Mahadevan, A., Thomsen, S. & Richards-Kortum, R. R. (1994) *Gynecol. Oncol.* **52**, 31–38.
16. Richard-Kortum, R. R., Rava, R. P., Fitzmaurice, M., Tong, L. L., Ratliff, N. B., Kramer, J. R. & Feld, M. S. (1989) *IEEE Trans. Biomed. Eng.* **36**, 1222–1232.
17. Eyre, D. R., Koob, K. J. & Van Ness, K. P. (1984) *Anal. Biochem.* **137**, 380–388.
18. Harbig, K., Chance, B., Kovac, A. G. B. & Reivich, M. (1976) *J. Appl. Physiol.* **41**, 480–488.
19. Deyl, Z., Macek, K., Adam, M. & Vancikov, A. (1980) *Biochim. Biophys. Acta* **625**, 248–254.
20. Bessey, O. A., Lowry, O. H. & Love, R. H. (1949) *J. Biol. Chem.* **180**, 755–769.
21. Richards-Kortum, R. R., Rava, R. P., Petras, R. E., Fitzmaurice, M., Sivak, M. V. & Feld, M. S. (1991) *Photochem. Photobiol.* **53**, 777–786.